



HAL
open science

On embedded microwave imaging systems: retrievable information and design guidelines

Lorenzo Crocco, Amelie Litman

► **To cite this version:**

Lorenzo Crocco, Amelie Litman. On embedded microwave imaging systems: retrievable information and design guidelines. *Inverse Problems*, 2009, 25 (6), pp.065001. 10.1088/0266-5611/25/6/065001 . hal-00438270

HAL Id: hal-00438270

<https://hal.science/hal-00438270>

Submitted on 5 Nov 2018

HAL is a multi-disciplinary open access archive for the deposit and dissemination of scientific research documents, whether they are published or not. The documents may come from teaching and research institutions in France or abroad, or from public or private research centers.

L'archive ouverte pluridisciplinaire **HAL**, est destinée au dépôt et à la diffusion de documents scientifiques de niveau recherche, publiés ou non, émanant des établissements d'enseignement et de recherche français ou étrangers, des laboratoires publics ou privés.

On embedded microwave imaging systems: retrievable information and design guidelines

Lorenzo Crocco¹ and Amélie Litman²

¹ CNR - IREA; National Research Council - Institute for Electromagnetic Sensing of the Environment, 328 via Diocleziano, 80124, Napoli, Italy

² Institut Fresnel, Aix-Marseille Université, CNRS, Ecole Centrale de Marseille, Campus de Saint-Jerôme, 13397 Marseille Cedex 20, France

E-mail: crocco.l@irea.cnr.it, amelie.litman@fresnel.fr

Abstract. In several applications, microwave imaging systems are enclosed in a dielectric or metallic casing, which is aimed at hosting a matching fluid and/or enabling a “removal” of the parasitic interactions with the surrounding environment. In order to understand which are the expected results of an imaging process carried out in such a configuration, in this paper we study the spectral properties of the integral radiation operator relative to an imaging system hosted in a circular metallic cavity. The analysis allows us to explain the role of the several parameters coming into play in the design of such a system, as well as their effect on the imaging procedure.

1. Introduction

Microwave imaging techniques have been a topic of active research in the last years. Indeed, researchers from many groups in the world have spent their efforts in developing several inversion techniques and providing evidences of their actual feasibility for quantitative imaging purposes. An almost comprehensive overview on these results is for instance given in some special sections published by this journal [1, 2, 3].

With respect to this context, besides the interest in developing new approaches and algorithms, there is a growing need of making the approaches suited to the practical conditions actually faced in the applications. This is for instance the case of subsurface imaging via Ground Penetrating Radar, wherein the modification of the radiation pattern of the antenna is important for the correct setting of the inversion [4].

Another example, which is of interest in biomedical applications and non-destructive testing, is the one in which the imaging system is immersed in a matching fluid aimed at improving the coupling between the target under test and the probing wave [5, 6, 7, 8, 9, 10]. In such a case, the overall system is enclosed in a casing, either dielectric or metallic, needed to confine the fluid and helpful in shielding or at least controlling the electromagnetic interactions between the imaging system and the surrounding environment. Of course, the presence of the casing must be properly taken into account in the imaging procedure [5, 11, 12, 13, 14], but it is also of importance to understand which constraints on the design of the overall imaging system are introduced by its presence. In addition, it is of interest to understand the effect of the presence of an embedding on the performances of the imaging procedures. It is worth to note that, the proper design of such a system is nowadays an issue of extreme relevance, since this kind of devices are the mostly considered ones in microwave diagnostics for breast cancer, probably the most promising and challenging context for inverse scattering based microwave imaging methods [8, 10].

Nevertheless, to the best of our knowledge, a systematic study of the factors which arise in this context has not been carried out yet, even in canonical configurations. For instance, it seems still not clear at all if and to what extent the imaging system may benefit from the presence of the casing [11, 14]. With respect to such a framework, the aim of this paper is to study the case of a two-dimensional circular scanning system embedded in a metallic casing. It is worth to note that this configuration corresponds to an actual device, which has been realized and exploited [5, 6, 15].

In order to pursue the above aim, we take advantage of an analysis of the properties of the *radiation* operator that relates the induced contrast sources to the scattered fields. In particular, by computing its singular value decomposition [16], we investigate the number of degrees of freedom (NDF) [17] pertaining to this linear operator. As well known, the NDF provides a convenient tool to understand those features of the inverse scattering problem which are of interest in the design of the imaging system, that is:

- (i) the minimum number of independent measurements needed to correctly perform the experiment;

- (ii) the amount of parameters which can be reliably extracted from the inversion of data (in the lack of any other a priori information);
- (iii) the “class” of unknown functions which can be reconstructed in the imaging process.

Therefore, a study of the NDF allows to assess both the *quantity* and the *quality* of the information available in the inverse problem at hand. As it will be shown, in the specific case considered, these features are influenced by the various parameters that come into play (e.g., the working frequency, the position of the probes, the size of the metallic casing and of the targets), so that the provided analysis will give an insight on how to properly choose these quantities with respect to the performance of an imaging procedure carried out in an embedded set-up.

It is worth to remark that the study of the NDF of the relevant linear operator has been widely adopted in the literature to address the problem of characterizing the information content of an inverse problem, meant as the number of parameters and the class of functions which can be reliably retrieved. For instance, this tool has been exploited to study the features of the linear inverse scattering problem in the canonical free space configuration [18, 19, 20], in the subsurface or aspect-limited geometries [21, 22], as well as to study the inverse source problem in nonhomogeneous backgrounds or in presence of unconventional media [23, 24]. It is also worth noting that the information content of the inverse problem at hand could be also instigated by exploiting a statistical framework based on the Fisher information analysis [25, 26].

The paper is organized as follows. In section 2 the scattering problem underlying an imaging system hosted in a perfectly conducting casing is formulated with respect to the two-dimensional scalar case (TM polarization). Section 3 is devoted to briefly recall the properties of the radiation operator in the canonical idealized situation, in which the system is hosted in an unbounded medium. Section 4 introduces the singular system of the radiation operator as valuated in the presence of the embedding, while section 5 investigates the role of the factors that affect the spectral properties of this latter, in order to address the choice of these parameters in the design of the imaging system. Once that these tools have been assessed, the comparison of the expected performances of an embedded imaging system versus those of an “unbounded” one is discussed in section 6. Concluding remarks follows.

2. Formulation and tools

2.1. Description of the problem

The imaging system configuration which will be considered in the following is depicted in figure 1. The system (made by the scatterer and the probes) is enclosed in a metallic casing of circular cross-section Σ having radius R_Σ that is filled with a medium Ω_b having (complex) permittivity $\varepsilon_{rb} = \varepsilon'_{rb} - i\varepsilon''_{rb}$. All the considered materials are assumed to be non-magnetic, hence the magnetic permeability is everywhere equal to that of vacuum, μ_0 . An array of time-harmonic ideal 2D point sources, that is elementary

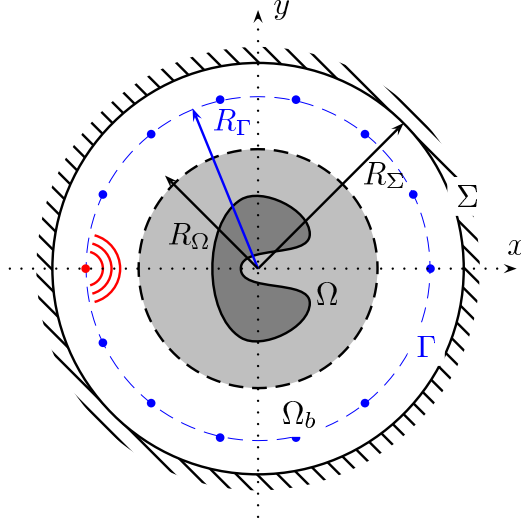


Figure 1. Cross-section of the imaging system enclosed in a cavity. The metallic border Σ has a circular cross-section of radius R_Σ . The emitters and receivers are placed within the cavity on the circular probing line Γ . The investigation domain Ω is also circular, it is placed at the center of the setup and encloses the unknown targets that have arbitrary cross-sections.

current distributions infinitely extended along the z -axis, is placed on a circle Γ with radius R_Γ and exploited to produce the primary field and measure the scattered field due to a set of non-magnetic targets having arbitrary cross-section and of infinite extent along the z direction. These latter are located at the center of the setup, within a cylindrical volume of circular cross-section Ω with radius R_Ω .

By assuming and omitting the time factor $\exp(i\omega t)$, the propagation problem can be modeled as a scalar one, owing to the invariance properties, and cast as the pair of equations:

$$E^s(\vec{r}) = k_b^2 \int_{\Omega} G(\vec{r}, \vec{r}') E^t(\vec{r}') \chi(\vec{r}') d\vec{r}', \quad \vec{r} \in \Gamma \quad (1)$$

$$E^t(\vec{r}) = E^i(\vec{r}) + k_b^2 \int_{\Omega} G(\vec{r}, \vec{r}') E^t(\vec{r}') \chi(\vec{r}') d\vec{r}', \quad \vec{r} \in \Omega \quad (2)$$

where $k_b = \omega \sqrt{\varepsilon_{rb} \mu_0}$ is the wavenumber in the host medium Ω_b at the pulsation ω , and E^i , E^t and E^s are the z -components of the field radiated from the primary sources, the total field induced by this latter inside the targets and the field scattered by the objects under test on Γ , respectively. The function

$$\chi(\vec{r}) = \frac{\varepsilon_r(\vec{r})}{\varepsilon_{rb}} - 1 \quad (3)$$

defines the “contrast” between the host medium permittivity and that corresponding to the targets embedded in Ω , $\varepsilon_r(\vec{r}) = \varepsilon'_r(\vec{r}) - i\varepsilon''_r(\vec{r})$.

The kernel $G(\vec{r}, \vec{r}')$ of the integral equations (1),(2) is the Green function of the problem that expresses the field of an elementary source located in $\vec{r}' = (\rho', \theta')$ as observed in the point $\vec{r} = (\rho, \theta)$. In the considered configuration, it has been shown that

such a function can be expressed as a single summation of Bessel functions [5, 12] as:

$$G(\vec{r}, \vec{r}') = \frac{1}{4} \sum_{n=-\infty}^{+\infty} \frac{J_n(k_b \rho_{<})}{J_n(k_b R_\Sigma)} [Y_n(k_b R_\Sigma) J_n(k_b \rho_{>}) - J_n(k_b R_\Sigma) Y_n(k_b \rho_{>})] e^{in(\theta - \theta')} \quad (4)$$

where $\rho_{<} = \min(\rho, \rho')$ and $\rho_{>} = \max(\rho, \rho')$ and J_n, Y_n denote the first and second kind Bessel functions of order n , respectively.

2.2. Field properties via spectral analysis

As long as one is interested in understanding the properties of the fields in the considered configuration, it proves convenient to rewrite (1) in an operator formalism. To this aim, let us denote with $J(\vec{r}) = \chi(\vec{r}) E^t(\vec{r})$ the contrast source induced by the incident field in Ω and define the integral operator:

$$\mathcal{A} : J \in L^2(\Omega) \rightarrow E^s \in L^2(\Gamma) = k_b^2 \int_{\Omega} G(\vec{r}, \vec{r}') J(\vec{r}') d\vec{r}', \quad (5)$$

that relates the current induced in the investigated region to the field scattered by the anomalies therein located as evaluated at the receivers locations. Owing to the Green's function properties, the *radiation* operator \mathcal{A} is compact, so that it can be represented through its singular value decomposition (SVD) as [16]:

$$\mathcal{A}(J)(\vec{r}) = \sum_{n=-\infty}^{+\infty} \sigma_n \langle J | v_n \rangle_{\Omega} u_n(\vec{r}) \quad (6)$$

where the scalar product on Ω is defined by

$$\langle f | g \rangle_{\Omega} = \int_{\Omega} f(\vec{r}) g^*(\vec{r}) d\vec{r}, \quad (7)$$

with g^* denoting the complex conjugate of g .

In eq.(6), $\{\sigma_n\}$ are the singular values ordered for decreasing magnitude and accumulating to zero for $n \rightarrow \infty$, while $\{v_n\}$ and $\{u_n\}$ correspond to the singular functions. In particular, the left-hand singular functions u_n provide a basis for the space of the scattered fields on Γ , while the right-hand ones, v_n , are a basis for the set of the radiating part of the contrast sources defined on Ω .

Now, the properties of the scattered fields can be inferred from the SVD equation (6). As a matter of fact, the decaying behavior of the singular values introduces a spectral cut-off that essentially defines the dimension of the scattered field's space. This in turn fixes the number of degrees of freedom of the field [17], that identifies the number of parameters needed to represent the field, within a given accuracy, as well as the number of basis functions that contribute in a meaningful way to the radiation of the (induced or impressed) sources J . The span of these latter identifies the allowable spatial content for a radiating contrast source and therefore it is useful in defining the class of retrievable contrast functions in the inversion procedure [19, 22, 21, 20].

It is worth to explicitly note that, due to reciprocity and due to the fact that the receiving and transmitting probes are located on the same curve, the study of the singular system of \mathcal{A} also determines the number of independent scattering experiments that can be realized with the imaging system at hand, as well as the kind of incident fields that can be induced by means of the adopted set-up.

3. Field properties in the unbounded medium configuration

For the sake of clarity, we briefly recall in this Section the well known results concerning the radiation operator in the canonical unbounded medium configuration [18, 19, 20].

In this configuration, which corresponds to removing the metal casing present in figure 1 and thus considering the medium Ω_b to be unbounded, the singular system is given by [19]:

$$v_n^u(\vec{r}') = c_n^u [J_n(k_b \rho')]^* \exp(in\theta') \quad (8)$$

$$u_n^u(\vec{r}) = d_n^u H_n^{(2)}(k_b R_\Gamma) \exp(in\theta) \quad (9)$$

$$\sigma_n^u = \frac{1}{c_n^u d_n^u}, \quad (10)$$

$H_n^{(2)}$ being the second kind Hankel function of order n and

$$c_n^u = \left(2\pi \int_0^{R_\Omega} |J_n(k_b \rho')|^2 \rho' d\rho' \right)^{-1/2} \quad (11)$$

$$d_n^u = \left(2\pi R_\Gamma |H_n^{(2)}(k_b R_\Gamma)|^2 \right)^{-1/2}, \quad (12)$$

where the superscript u is meant to recall that an *unbounded* medium is being considered. Note that, for a fixed position of the observation domain R_Γ , the singular functions u_n^u only depend on the angular variable.

From the analysis of this singular system, the following main observations arise:

- when primary sources and measurement probes are placed at some wavelengths apart from the object under test, the field can be represented, within a given accuracy, with a finite number of parameters [18, 17];
- if the scatterer is in size sufficiently large with respect to the wavelength, such a number only depends on the electrical dimension of the scatterer, whatever the required accuracy [18, 17];
- an increase in the number of parameters (this time depending on the considered accuracy) can be induced by moving the probes, in the “close-proximity” of the scatterer. Such an enlargement can be explained by considering that the higher spatial frequency components of the fields are caught by the probes when positioned in the vicinity of the targets [19].

These observations provide some clues on the quantity of information that is associated with the measured field and that can be extracted in the inverse problem. Moreover, the singular functions also provide a characterization of the kind of incident fields that can be realized, as well as of the components of the contrast source that can be reconstructed. When a linear inverse scattering problem is dealt with, this knowledge directly furnishes a definition of the class of retrievable contrast functions, in both the single view and multi-view cases [17, 19, 20]. In the general non-linear case, no general result can be drawn. Nevertheless, the observation of the singular functions still provides some hints on the kind of retrievable functions [19].

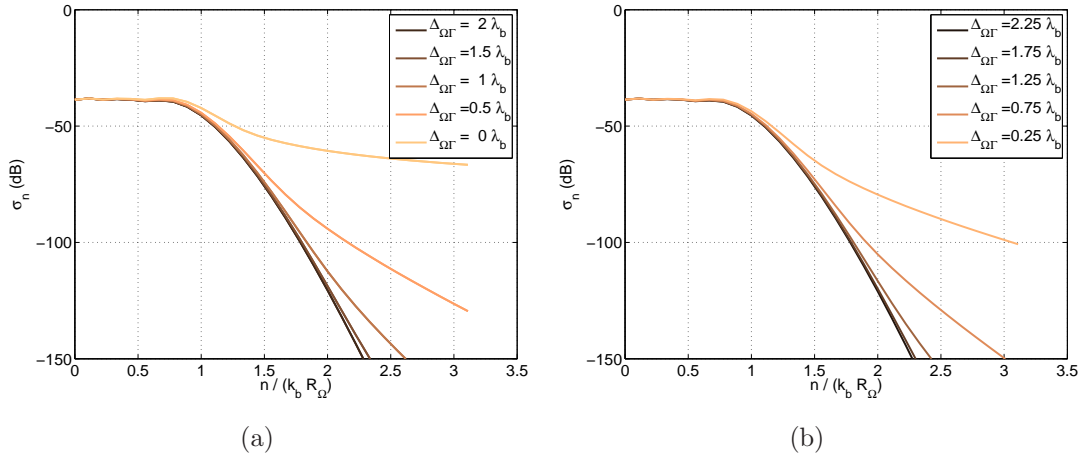


Figure 2. Singular spectrum in the unbounded medium configuration for several values of the distance $\Delta_{\Omega\Gamma}$. The probing line R_Γ is moving (a) with a step of $\lambda_b/2 + p\lambda_b/2$ from R_Γ^{max} , (b) with a step of $\lambda_b/4 + p\lambda_b/2$ from R_Γ^{max} . The embedding medium Ω_b is lossless.

In order to give an example of the above observations, let us observe figure 2, where it is reported the behavior of the singular values σ_n^u for a source domain $R_\Omega = 1.5\lambda_b$ hosted in a lossless medium, when varying the position of the probes R_Γ between $R_\Gamma^{min} = R_\Omega$ and $R_\Gamma^{max} = R_\Omega + 2.5\lambda_b = 4\lambda_b$. The wavelength of the embedding medium λ_b is given by $\lambda_b = 2\pi/k_b$. In particular, in panel (a) R_Γ is decreased with a step of $\lambda_b/2$ from R_Γ^{max} , while in panel (b) it is decreased with the same step but starting from $R_\Gamma^{max} - \lambda_b/4$. As it can be observed, for a fixed accuracy, the number of significant singular values depends on the distance $\Delta_{\Omega\Gamma} = |R_\Gamma - R_\Omega|$ [19]. As a matter of fact, when such a distance is larger than $\lambda_b/2$, the singular values have an almost identical decay regardless of the particular value. In particular, being the scatterer not extremely large, the number of significant singular values slightly depends on the considered accuracy, but it is always larger than $k_b R_\Omega$. On the other hand, when the probes approach the investigation area, the decay becomes slower and strongly depends on the position of the probes. Accordingly, the number of significant singular values strongly depends on the considered accuracy. It is worth noting that, in agreement with the physical intuition, this increase of the NDF does not entail a straightforward improvement of the achievable spatial resolution. As a matter of fact, as shown in [19], owing to the spatial properties of the singular functions associated with the “extra” above-threshold singular values, the resolution improvement is circumscribed to those parts of the domain under test that are actually in the near-field region of the probes.

In figure 3, we reported the behavior of the singular values σ_n^u in the same conditions as before, but assuming a lossy host medium having a loss tangent of $\tan(\delta) = \varepsilon''_{rb}/\varepsilon'_{rb} = 0.051$. In this case, the background wavelength of the embedding medium is defined as $\lambda_b = 2\pi/\Re(k_b)$. As it can be observed, while the presence of losses leaves unaltered both the “far-field” and “proximity” features of the singular values’ spectrum, it affects the overall spectrum level, which appears to be slightly attenuated

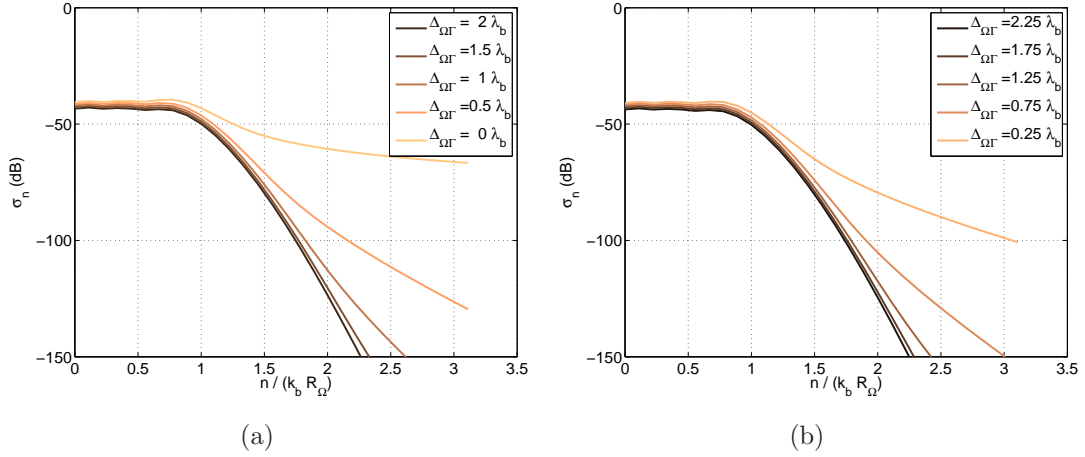


Figure 3. Singular spectrum in the unbounded medium configuration for several values of the distance $\Delta_{\Omega\Gamma}$. The probing line R_Γ is moving (a) with a step of $\lambda_b/2 + p\lambda_b/2$ from R_Γ^{max} , (b) with a step of $\lambda_b/4 + p\lambda_b/2$ from R_Γ^{max} . The embedding medium Ω_b is lossy, with a loss tangent of $\tan(\delta) = 0.051$.

when the distance between targets and probes increases.

4. Field properties in the embedded configuration

Let us now turn to the study of the singular system of the radiation operator \mathcal{A} pertaining to the embedded configuration. By exploiting similar tools as those used to compute the singular system in the unbounded medium case, it is possible to show that the associated singular system is given by (see appendix):

$$v_n(\vec{r}') = c_n [J_n(k_b \rho')]^* \exp(in\theta') \quad (13)$$

$$u_n(\vec{r}) = d_n \left[\frac{Y_n(k_b R_\Sigma) J_n(k_b R_\Gamma) - J_n(k_b R_\Sigma) Y_n(k_b R_\Gamma)}{J_n(k_b R_\Sigma)} \right] \exp(in\theta) \quad (14)$$

with

$$c_n = \left(2\pi \int_0^{R_\Omega} |J_n(k_b \rho')|^2 \rho' d\rho' \right)^{-1/2} \quad (15)$$

$$d_n = \left(2\pi R_\Gamma \left| \frac{Y_n(k_b R_\Sigma) J_n(k_b R_\Gamma) - J_n(k_b R_\Sigma) Y_n(k_b R_\Gamma)}{J_n(k_b R_\Sigma)} \right|^2 \right)^{-1/2} \quad (16)$$

and the singular values are still given by

$$\sigma_n = \frac{1}{c_n d_n}. \quad (17)$$

As it can be observed, several analogies and differences hold with respect to the previous case. In particular, as far as the singular functions are concerned, one can immediately notice that the right singular functions v_n and v_n^u coincide in the two cases, whereas the left singular ones u_n and u_n^u share the same dependance on the angular variable, consistently with the fact that the observation domain is the same, but are

weighted for different factors owing to the different boundary conditions arising in the cases considered.

When turning to the analysis of the singular spectrum, the first analogy which appears is that the factor c_n , which only depends on the electric dimension of the investigated region $k_b R_\Omega$, is exactly coincident with that of the unbounded medium configuration, c_n^u . As such, it will provide the aforementioned decay of the singular spectrum for $n > k_b R_\Omega$. Such a decay will be exponentially fast in the high frequency regime (i.e., for $k_b R_\Omega \gg 1$), while it will exhibit a slower rate when considering a region in size comparable or smaller than the wavelength.

In order to proceed with the analysis of the singular spectrum's properties, we have now to concentrate on the term d_n . To this aim, it is worth to first recall that the considered configuration can be seen, in the absence of the scatterer, as a resonant cavity, which will be therefore characterized by the eigenmodes provided by the solution of the following set of equations

$$\begin{cases} \Delta E(\vec{r}) + k_b E(\vec{r}) = 0 & \vec{r} \in \Omega_b \cup \Omega \\ E(\vec{r}) = 0 & \vec{r} \in \Sigma \end{cases} \quad (18)$$

Apart from the trivial null solutions, the eigenmodes for the considered geometry are of the form [27]

$$E_{n,m}(\vec{r}) = a_{n,m} J_n(k_{n,m} \rho) \exp(in\theta), \quad n \geq 0, m \geq 1 \quad (19)$$

with the condition that

$$k_{n,m} = \frac{j_{n,m}}{R_\Sigma}, \quad (20)$$

where $j_{n,m}$ corresponds to the m -th zero of the n -th Bessel function J_n .

In particular, for a given size of the embedding $k_b R_\Sigma$, there exist a finite number of pairs n, m such that the condition

$$\frac{j_{n,m}}{k_b} < R_\Sigma \quad (21)$$

is matched. This means that the associated eigenmodes are present in the cavity, since the corresponding Bessel function admits at least a zero inside the embedding. The largest order n_{max} that can be allowed is given by the condition

$$j_{n_{max},1} \leq k_b R_\Sigma < j_{n_{max}+1,1}. \quad (22)$$

5. Molding the singular spectrum through eigenmodes excitation

Some interesting observations can be done if the condition

$$\frac{j_{\tilde{n},\tilde{m}}}{k_b} = R_\Sigma \quad (23)$$

holds for some \tilde{n} and \tilde{m} , i.e., if, for a given dimension of the empty cavity, a Bessel function of order \tilde{n} exists, whose \tilde{m} -th zero *exactly* falls on the cavity border. Indeed, if this happens, the excited eigenmode coincides with the \tilde{n} -th singular function $v_{\tilde{n}}$.

Moreover, due to the fact that owing to (23) $J_{\tilde{n}}(k_b R_\Sigma) = 0$, it follows that the corresponding singular value becomes infinite. As a consequence, the spectrum of the operator \mathcal{A} has an abrupt modification with respect to the unbounded medium case depicted in figure 2, as it will only present a very large (infinite, actually) singular value which will dominate all the others, becoming the only significant contribution to the data in the inverse problem.

However, by observing the expression of d_n in (16), one can understand that this circumstance can be avoided by properly positioning the probing/observation circle R_Γ . Indeed, by choosing this latter in such a way that R_Γ exactly falls on a \tilde{p} -th zero of $J_{\tilde{n}}$, i.e., $J_{\tilde{n}}(k_b R_\Gamma) = 0$, of course under the constraint $\tilde{p} < \tilde{m}$, i.e., $R_\Gamma < R_\Sigma$, it follows that the considered eigenmode is still excited, but the corresponding singular value attains a finite value, i.e.,

$$\sigma_{\tilde{n}}^2 = \frac{2\pi R_\Gamma}{c_{\tilde{n}}} \times |Y_{\tilde{n}}(k_b R_\Gamma) + Y_{\tilde{n}}(k_b R_\Sigma)| \prod_{k=1, k \neq \tilde{m}, k \neq \tilde{p}}^{\infty} \frac{j_{\tilde{n},k}^2 - j_{\tilde{n},\tilde{p}}^2}{j_{\tilde{n},k}^2 - j_{\tilde{n},\tilde{m}}^2} |^2. \quad (24)$$

By doing so, it is possible therefore to *mold* the spectrum of the operator by properly enhancing the contribution of a specific singular function, through the increase of the corresponding singular value. In particular, since the singular values are by definition ordered in a decreasing fashion, this means that the choice of the design parameters of the embedded system (i.e., working frequency, embedding medium, R_Σ and R_Γ) introduces a modification in the ordering of the singular functions with respect to the unbounded configuration, thus actually modifying the class of “retrievable” functions in the inversion.

The previous considerations were drawn by considering that the size of the embedding was exactly matching a zero of a particular Bessel function and assuming a purely dielectric embedding medium. However these conditions, especially the latter, are seldom satisfied in the applications, so that it is of interest to understand if and to what extent the above observations apply.

To this aim, note that, when a lossy medium is considered and/or when condition (23) is not met, nevertheless, owing to (21), several eigenmodes will be present in the embedding. In particular, these latter will exactly coincide (in the imaged region) with the singular functions v_n corresponding to the relevant Bessel functions.

Now, by observing the expression of d_n (16), one can understand that the singular values corresponding to these particular singular functions will be more or less enhanced depending on the relative distance of the zero of the pertaining singular function from the cavity border, as this parameter directly influences the denominator of d_n , i.e., $J_n(k_b R_\Sigma)$. As a consequence, even in this case, it is possible to properly act on the spectral content of the singular functions span by means of a convenient ordering of the sequence of the zeros.

However, it must be recalled that R_Σ is not the only quantity that comes into play. As a matter of fact, one must take also into account the effect of the probing line position R_Γ on which the factor d_n depends in a periodic way, with a different periodicity for different values of the index n .

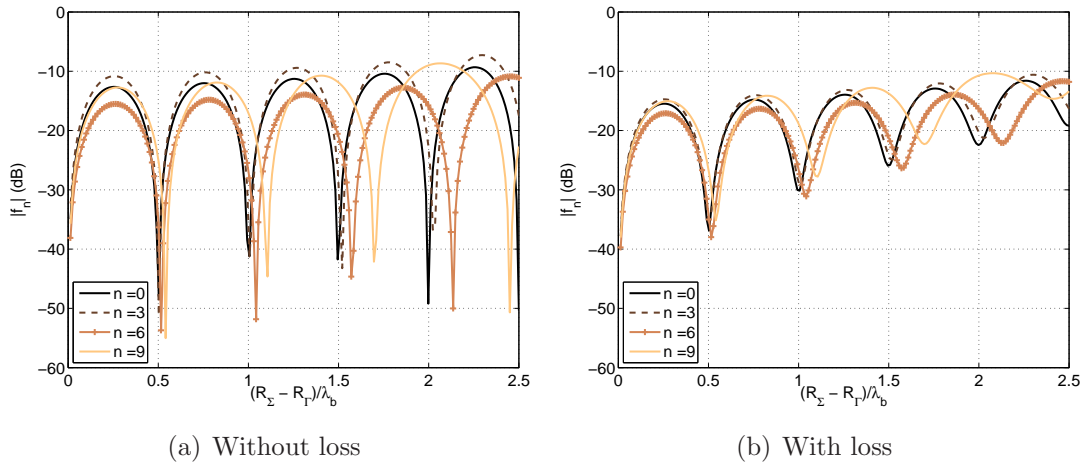


Figure 4. Evolution of the amplitude of f_n with respect to the distance between the probing line R_Γ and the metallic casing, R_Σ . The external medium is (a) lossless or (b) with a loss tangent of $\tan(\delta) = 0.051$.

In particular, it is useful to observe the behavior of the amplitude of

$$f_n(\rho) = \frac{Y_n(k_b R_\Sigma) J_n(k_b \rho) - J_n(k_b R_\Sigma) Y_n(k_b \rho)}{J_n(k_b R_\Sigma)}, \quad (25)$$

as a function of the distance $R_\Sigma - R_\Gamma$. For some values of n , a plot of this latter is given, for both the lossless and lossy cases, in figure 4. As it can be noticed, for all the indices, $f_n(\rho)$ reaches a maximum of the amplitude for $R_\Sigma - R_\Gamma = \lambda_b/4$ and a minimum amplitude for $R_\Sigma - R_\Gamma = \lambda_b/2$. As a consequence, whatever the choice of the casing size R_Σ (which entails a particular ordering of the singular functions), when the probing line is placed at $R_\Sigma - R_\Gamma = \lambda_b/2$, the singular value spectrum will be lowered. Clearly this does not happen if $R_\Sigma - R_\Gamma = \lambda_b/4$, so that, provided this condition is fulfilled, it follows that it is still possible to selectively enhance the singular values by fixing the size of the embedding. It is also worth to note that when the distance becomes larger than $\lambda_b/2$, the periodicity of the extremal points of (25) is not the same for all the values of n , so that the effect is not anymore easily predictable. Accordingly, $R_\Sigma - R_\Gamma = \lambda_b/4$ appears as convenient practical choice.

A simple physical explanation of the above findings is that, when considering a source located in the imaged domain Ω , the interaction between this latter and the casing gives raise to different destructive and constructive patterns. Therefore, depending on the observation line's position, different field levels can be detected. Exploiting reciprocity arguments, this also suggests that the probing line has to be properly positioned (i.e., in a location corresponding to a constructive interference), in order to provide a meaningful incident field in the imaged region. Of course, such an effect will be generally smoothed when losses are present in the host medium Ω_b .

5.1. A practical example

In order to observe the above described effects, we have evaluated the singular spectrum in the same cases considered in the unbounded configuration, section 3, assuming that the metallic boundary is located at $R_\Sigma = R_\Gamma^{max} = 4\lambda_b$. The results obtained for the case in which the host medium Ω_b is lossless are shown in figure 5.

Some comments are now in order.

- First, note that the spectra are ordered according to the indices of the pertaining Bessel function. By so doing, one can indeed appreciate the “selective enhancement” effect induced by the presence of the casing.
- It can also be noticed that, as expected, the spectra are different depending on the relative position of the probing line with respect to the casing. As a matter of fact, for values of n below $k_b R_\Omega$, when the probing line is placed in such a way that $R_\Sigma - R_\Gamma$ is a multiple of $\lambda_b/2$, the amplitude of the “low order” singular values is generally lowered, whereas, when $R_\Sigma - R_\Gamma$ is a multiple of $\lambda/4$, this does not happen.
- When $R_\Sigma - R_\Gamma$ is a multiple of $\lambda/2$, the low order singular values increase when approaching the boundary of the investigated region R_Ω . This is due to the increase of the minima of (25) as well as to the different periodicity of its extremal points, see figure 4.
- Conversely, for values of n above $k_b R_\Omega$, all the spectra exhibit a very similar behavior, since they are basically dominated by the factor c_n , which is independent of the set-up parameters (R_Σ and R_Γ).
- It is worth to observe that, for $n > k_b R_\Omega$, an increase or a decrease of some singular values can still be observed, as long as the probes are far from the investigation domain. In the close proximity case (i.e., when $R_\Gamma \rightarrow R_\Omega$), no specific singular value is enhanced. This circumstance is due to the fact that probes positioned close to the domain do not intersect the zeros of the high order Bessel functions (that are relevant to that part of the spectrum), which are indeed located in the vicinity of the metallic casing.

In figure 6, the same situation as before has been considered, but for the presence of losses in the embedding medium Ω_b . As it can be noticed, despite the obvious smoothing introduced by the attenuation, still similar considerations as those done in the previous case hold true.

For the considered geometry, it is also interesting to observe the displacement of the zeroes of the Bessel functions, since their ordering with respect to their distance from the embedding exactly provides the “molding” rule for the singular values and functions. This circumstance is shown in figure 7(a), wherein it is reported the position of the zeroes of the first 8 eigenmodes that fall close to the boundary. As it can be seen by comparing figure 7(b) and figure 5(b), the eigemode’s zero distance from the border is exactly proportional to the magnitude of the singular values.

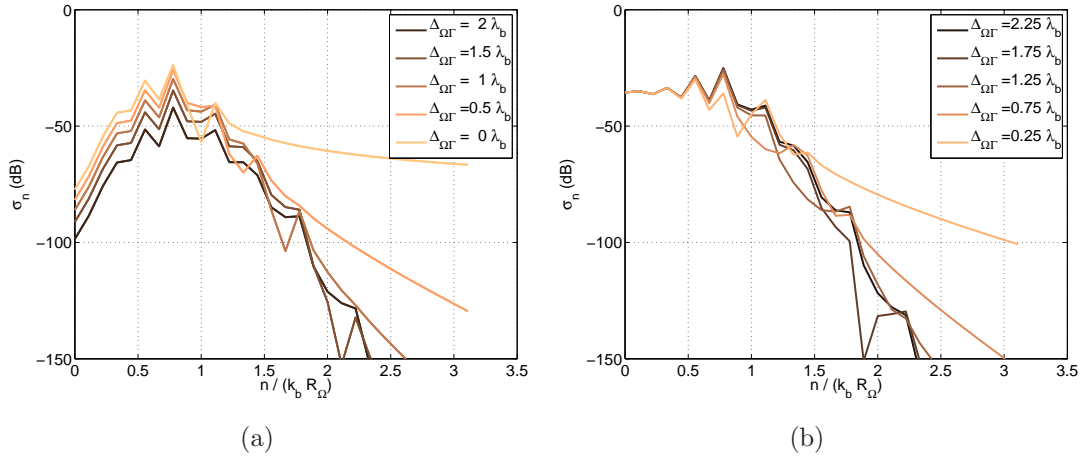


Figure 5. Singular spectrum for the embedded configuration with $R_\Sigma = 4\lambda_b$, $R_\Omega = 1.5\lambda_b$ and different values of $\Delta_{\Omega\Gamma}$. The probing line moves (a) with a step of $\lambda_b/2 + p\lambda_b/2$ from R_Σ or (b) with a step of $\lambda_b/4 + p\lambda_b/2$ from R_Σ . The embedding medium is lossless.

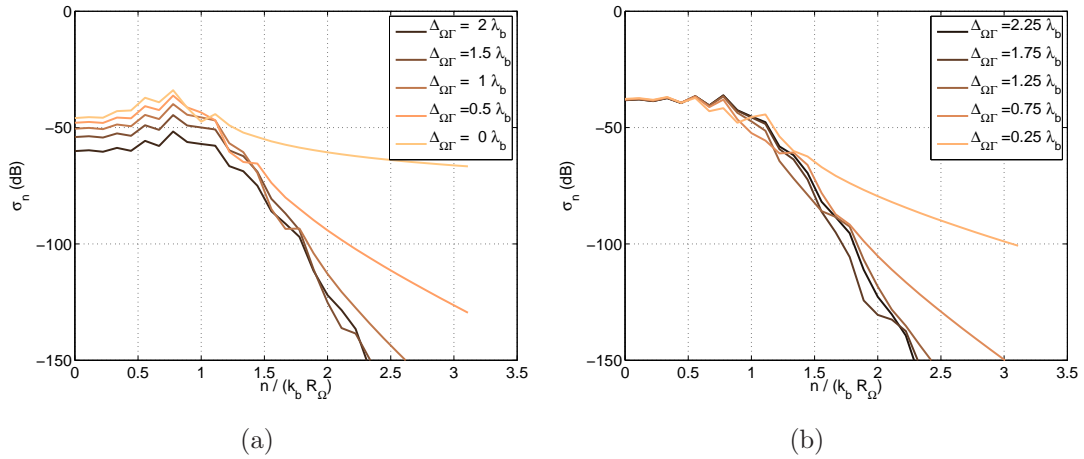


Figure 6. Singular spectrum for the embedded configuration with $R_\Sigma = 4\lambda_b$, $R_\Omega = 1.5\lambda_b$ and different values of $\Delta_{\Omega\Gamma}$. The probing line moves (a) with a step of $\lambda_b/2 + p\lambda_b/2$ from R_Σ or (b) with a step of $\lambda_b/4 + p\lambda_b/2$ from R_Σ . The embedding medium is lossy, with a loss tangent of $\tan(\delta) = 0.051$.

5.2. A simple tool to design the imaging set-up

According to the above observations, it follows that a simple and useful tool to design an embedded imaging system like the one at hand is constituted by the plot shown in figure 8, wherein the sequence of the zeros of several Bessel functions in normalized coordinates is reported. As a matter of fact, by just entering the ordinate of this plot with a value of R_Σ normalized to the wavelength, it is possible to immediately draw the ordering of the corresponding singular values. By so doing, one can then foresee which are the singular functions onto which the most part of the field (if the u_n are concerned) or the contrast source (if the v_n are considered) is projected. Then, depending on which of the two conditions (21) or (23) is being fulfilled, the probing line has to be positioned

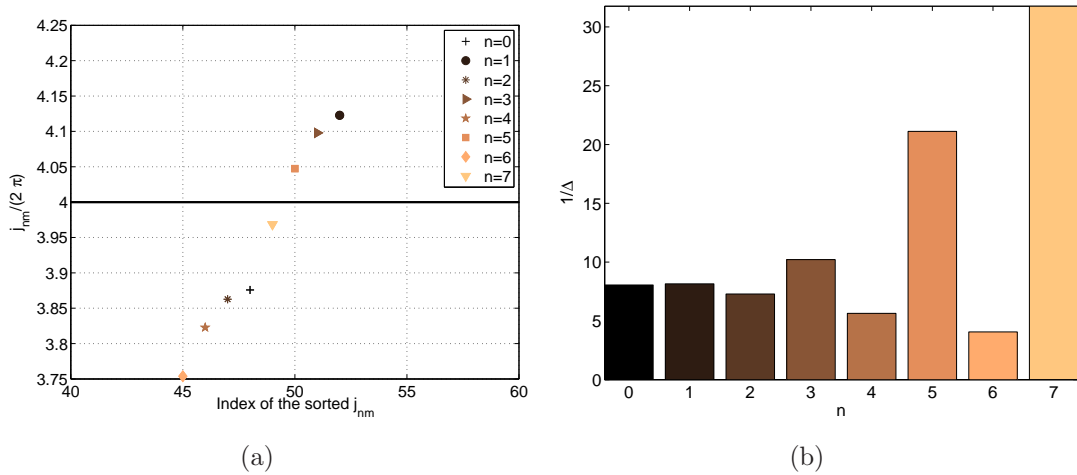


Figure 7. (a) Position of the zeroes of the first 8 eigenmodes which are located in the vicinity of $R_\Sigma = 4\lambda_b$ (b) Ordering of the eigenmodes with respect to $1/\Delta$, where $\Delta = |j_{nm}/(2\pi) - R_\Sigma/\lambda_b|$, m being the index of the zero of J_n which is closest to R_Σ/λ_b .

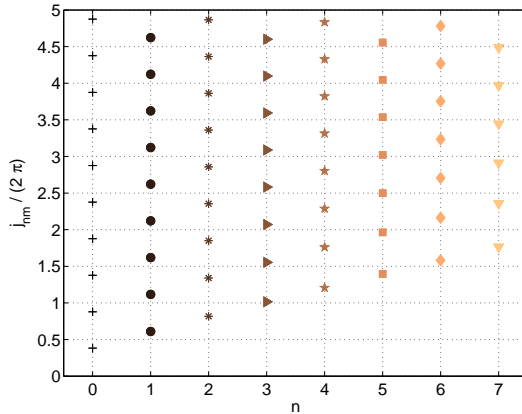


Figure 8. A simple abacus for the design of the embedded imaging system.

either on a zero of the Bessel function supporting the excited eigenmode or at a distance of $\lambda_b/4$ from the casing.

6. Some considerations on embedded vs. unbounded imaging systems

The analysis and the tools described in the previous section can be of help in trying to address a question which naturally comes to mind, i.e., how the presence of the metallic embedding affects the imaging process with respect to the corresponding unbounded situation. To this end, let us again consider the particular set-up described in the example of the previous sections. Although this is of course a particular case, it allows us to draw some general conclusions, thanks to the results achieved in section 5.

In figure 9, we have reported the singular values spectra in the two cases (unbounded and embedded), for several positioning of the probing line (away from the targets and

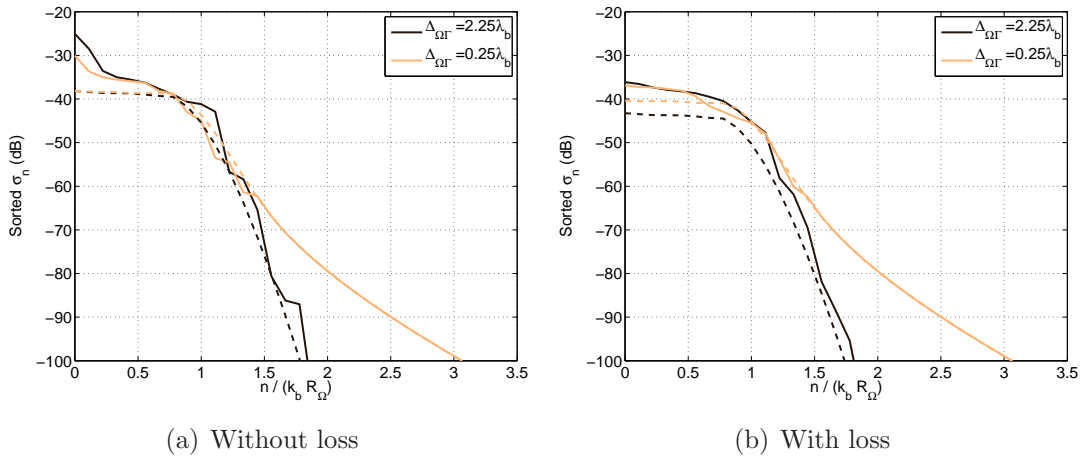


Figure 9. Comparisons of the unbounded configuration (dashed line) and the embedded configuration (full line) spectra for two positions of the receiving line. The target is located inside the domain Ω of radius $R_\Omega = 1.5\lambda_b$ and the casing, if present, is located at $R_\Sigma = 4\lambda_b$. The embedding medium is either (a) lossless or (b) with some losses with a loss tangent of $\tan(\delta) = 0.051$.

in the close proximity) and considering a lossless/lossy host medium Ω_b . Note that, unlike the previous plots, the singular values have been properly ordered in the case of the embedded system, in order to make a fair comparison between the spectra.

A first feature to notice is that the general trend of the singular values in either the transition ($n \approx k_b R_\Omega$) and the asymptotic regions is the same for both cases. This outcome, which is not surprising, being dictated by the factor c_n that is common to both σ_n and σ_n^u , entails that the amount of independent information carried by the fields is the same in the two configurations. Hence, *no modification of the quantity of available independent information* is introduced by considering a properly designed embedded imaging system.

Conversely, it appears that a different signal energy pertains to the two cases (i.e., the area subtended by the spectrum curve). As it can be observed, when the embedding and probing line are properly selected, the energy is larger in the presence of the casing, than in the unbounded configuration. This circumstance is physically related to the constructive interactions between the sources (primary or induced) and the casing and entails that a larger signal-to-noise ratio is expected when the imaging system is properly embedded. As a consequence, the imaging process in this configuration can be either more stable against the unavoidable uncertainties on the measured data and/or lead to the stable retrieval of a (slightly) larger number of spectral components when considering a fixed accuracy level. On the other hand, if the design of the embedding is not fulfilling the given criteria concerning the probing line positioning, the spectrum pertaining to the embedded configuration can be lower than the unbounded one.

A further difference can be pointed out recalling that, while the singular value index of the unbounded case corresponds to a singular function containing a Bessel function and a complex exponential of the same order, this is not the case for the embedded

system configuration, in which the ordering is dictated by the relative position of the zeroes of the eigenmodes with respect to the casing. For instance, in the lossless case, this could mean that most part of the energy can be associated with large order Bessel functions, rather than with the low order ones. This circumstance entails that, even if the *quantity* of information is the same in the two cases, the molding of the spectrum allows for a change in the *quality* of the retrievable information.

As far as the imaging process is concerned, it is worth to note that such a circumstance is not necessarily leading to an improvement, due to the spatially inhomogeneous behavior of the Bessel functions over the imaged domain Ω . As a matter of fact, when the index of the Bessel function (and of the pertaining exponential) grows, the corresponding singular function exhibits increasingly faster angular oscillations confined on the border of Ω . This also means that the corresponding incident field is almost vanishing in the center of the imaged domain. In the simple case in which the Born approximation holds true, wherein the contrast source is linearly related to the incident field as $J(\vec{r}) = \chi(\vec{r})E_{inc}(\vec{r})$, this entails that when the target support occupies only the center of the imaged region, a weaker, almost negligible, current will be induced on it, thus making it more difficult or even impossible to retrieve. This circumstance explains the finding based on numerical observations done in [14], where a similar kind of target (i.e. concentrated in the center of the imaged area) is better reconstructed when probing it under the unbounded configuration than when using the embedded system. On the other hand, our analysis also suggests that, under the same conditions, a target located on the border of the domain Ω will be more easily and accurately retrieved by adopting the embedded configuration. Examples of such behavior can be found in [28].

In the general case in which the Born approximation does not hold true, the reasoning cannot be as straightforward. However, it can be expected that similar results are found, since the singular functions still provide a basis for the contrast source. Hence, the circumstance under which the projection of the contrast source onto the leading singular functions is almost negligible in some part of the domain can indeed affect the result of the imaging process.

7. Conclusion

Owing to the growing interest towards embedded microwave imaging system, in this paper we have studied a configuration in which the system is enclosed in a circular metallic casing, with the goal of understanding the expected features of an imaging process performed in such an environment.

By taking advantage of the analysis of the number of degrees of freedom of the relevant radiation operator, we have shown that, with respect to the canonical unbounded medium configuration, there is no change in the *quantity* of available independent information that can be exploited in the inverse problem. Conversely, the *quality* of this information is different, due to the fact that the geometrical parameters of the set-up (i.e., the electric dimension of the embedding and the position of the probing

line) may lead to an enhancement of some singular functions with respect to others. Accordingly, we have recognized that by properly designing, by means of simple tools, the resonances of the embedding, it is possible to modify to some extent the class of retrievable contrast functions. Interestingly, our findings provide an explanation for the numerical observations reported in [14, 28] and appear in agreement with the practical criteria adopted in the actual realization of a system like the one considered in [5].

It is worth to remark that the similarities which have been pointed out between the SVD of the radiation operator for the embedded system considered in this paper and that of operator relevant to the canonical unbounded case allows us to easily extend the achieved results to the inverse scattering problem under multiple incidences, taking advantage of the results in [20]. Moreover, it is also interesting to notice that the capability of molding the spectrum of the operator that we have observed is in agreement with the considerations reported in the literature concerning the possible radiation enhancement achieved by means of a suitably designed metamaterial's substrate [24].

The present analysis does not deal with another parameter of importance in the solution of the inverse scattering problem, that is the non-linearity of the relationship between the data and the unknowns. As a matter of fact, it is known that the scenario plays a major role on determining the *degree of non-linearity* [29, 30] of the inverse scattering problem, so that further differences may arise between the embedded configuration and the unbounded one. As such, future work will be concerned with the evaluation of the non-linearity of the inverse scattering problem solved in an embedded configuration, along the lines traced in [29, 30].

In addition, the study of systems embedded in non-circular and/or non-metallic casing will be tackled, by exploiting suitable numerical procedures capable of achieving the Green's function that pertains to the considered geometries.

Appendix

When the Green's function is the product of two functions of separate variables in terms of ρ and θ , the singular values are always given by the inverse product of the weighting coefficients c_n and d_n of the singular functions.

In order to show this result, let us assume that the Green's function is of the following form:

$$G(\vec{r}, \vec{r}') = \sum_{n=-\infty}^{+\infty} A_n(\rho) e^{in\theta} B_n(\rho') e^{-in\theta'} \quad (26)$$

where the functions A_n and B_n are depending on the configuration at hand, $\vec{r} = (\rho, \theta)$ corresponds to the observation point and $\vec{r}' = (\rho', \theta')$ to the excitation point. The observation equation (1) can be rewritten as

$$E^s(\vec{r}) = \sum_{n=-\infty}^{+\infty} A_n(\rho) e^{in\theta} \int_{\Omega} J(\vec{r}') B_n(\rho') e^{-in\theta'} d\vec{r}' \quad (27)$$

$$= \sum_{n=-\infty}^{+\infty} A_n(\rho) e^{in\theta} \langle J(\vec{r}') | [B_n(\rho')]^* e^{in\theta'} \rangle_{\Omega} \quad (28)$$

where $J(\vec{r}')$ corresponds to the induced sources distribution inside the investigation domain Ω . By direct identification with (6), and due to the orthogonality properties of the exponential functions, we obtain

$$v_n(\vec{r}') = c_n [B_n(\rho')]^* e^{in\theta'} \quad (29)$$

$$u_n(\vec{r}') = d_n A_n(\rho) e^{in\theta} \quad (30)$$

where c_n and d_n are normalization coefficients in order to obtain a set of orthonormal singular functions. Thus, the coefficients c_n and d_n are given by

$$|c_n|^2 = 2\pi \int_0^{R_{\Omega}} |B_n(\rho')|^2 \rho' d\rho' \quad (31)$$

$$|d_n|^2 = 2\pi R_{\Gamma} |A_n(R_{\Gamma})|^2 \quad (32)$$

By rewriting (28) using the singular vectors notation, we obtain

$$E^s(\vec{r}) = \sum_{n=-\infty}^{+\infty} \frac{u_n(\vec{r}')}{d_n} \langle J | \frac{v_n}{c_n} \rangle_{\Omega} \quad (33)$$

By direct identification with (6), it follows that the singular values are given by

$$\sigma_n = \frac{1}{c_n d_n}. \quad (34)$$

In the free space case, the functions A_n and B_n are defined as

$$B_n(\rho') = J_n(k_b \rho'), \quad A_n(\rho) = H_n^{(2)}(k_b \rho). \quad (35)$$

In the casing case, the functions A_n and B_n are defined as

$$B_n(\rho') = J_n(k_b \rho'), \quad A_n(\rho) = \frac{Y_n(k_b R_{\Sigma}) J_n(k_b \rho) - J_n(k_b R_{\Sigma}) Y_n(k_b \rho)}{J_n(k_b R_{\Sigma})}. \quad (36)$$

Acknowledgments

This work has been performed while L. Crocco was visiting Institut Fresnel thanks to a visiting researcher grant from Ecole Centrale Marseille. A. Litman would also like to acknowledge the support of Agence Nationale pour la Recherche under the "Jeunes Chercheurs" grant no. JCJC06-141021 as well as the support of INTAS through the grant no. 06-1000017-8909.

- [1] K. Belkebir and M. Saillard. Special section: Testing inversion algorithms against experimental data. *Inverse Problems*, 17(6):1565–1571, 2001.
- [2] K. Belkebir and M. Saillard. Special section: Testing inversion algorithms against experimental data: inhomogeneous targets. *Inverse Problems*, 21(6):S1–S3, 2005.
- [3] Amelie Litman and Lorenzo Crocco. Testing inversion algorithms against experimental data: 3d targets. *Inverse Problems*, 25(2):020201 (5pp), 2009.
- [4] F. Soldovieri, R. Persico, and G. Leone. Effect of source and receiver radiation characteristics in subsurface prospecting within the DBA. *Radio Sci.*, 40:RS3006, 2005.
- [5] J.-M. Geffrin. *Imagerie microonde: Etude d'un scanner a 434 MHz pour des applications biomédicales*. PhD thesis, Univ. Paris XI, Orsay, France, 1995.
- [6] R. Lencrerot, A. Litman, H. Tortel, and J.-M. Geffrin. A microwave imaging circular setup for soil moisture information. In *IGARSS Conference Proc.*, pages 4394–4397, 2007.
- [7] L. Jofre, M. S. Hawley, A. Broquetas, E. De Los Reyes, M. Ferrando, and A. R. Elias-Fuste. Medical imaging with a microwave tomographic scanner. *IEEE Trans. Biomed. Eng.*, 37:303–311, 1990.
- [8] P. M. Meaney, K. D. Paulsen, A. Hartov, and R. K. Crane. An active microwave imaging system for reconstruction of 2-d electrical property distributions. *IEEE Trans. Biomed. Eng.*, 42:1017–1025, 1995.
- [9] A. Broquetas, J. Romeu, J. M. Rius, A. R. Elias-Fuste, A. Cardama, and L. Jofre. Cylindrical geometry: A further step in active microwave tomography. *IEEE Trans. Microwave Theory Tech.*, 39:836–844, 1991.
- [10] G.A. Ybarra, Q. H. Liu, J. P. Stang, and W. T. Joines. Microwave breast imaging. In J. S. Suri, R. Rangayyan, and S. Laxminarayan, editors, *Emerging Technology in Breast Imaging and Mammography*. American Scientific Publishers, USA/Canada, 2007.
- [11] A. Franchois and A.G. Tijhuis. A quasi-newton reconstruction algorithm for a complex microwave imaging scanner environment. *Radio Science*, 38:8011, 2003.
- [12] P. M. van den Berg and J. T. Fokkema. Removal of undesired wavefields related to the casing of a microwave scanner. *IEEE Trans. Microwave Theory and Tech.*, 51:187–192, 2003.
- [13] A.G. Tijhuis and A. Franchois. A two-dimensional microwave imaging algorithm for a complex environment: preliminary results. In *Proc. URSI Int. Electromagnetic Theory Symp.*, pages 445–447, 2001.
- [14] C. Gilmore and J. LoVetri. Enhancement of microwave tomography through the use of electrically conducting enclosures. *Inverse Problems*, 24(3):035008, 2008.
- [15] R. Lencrerot, A. Litman, H. Tortel, and J.-M. Geffrin. Imposing zernike representation for imaging two-dimensional targets. *Inverse Problems*, 25(3):035012 (18pp), 2009.
- [16] M. Bertero and P. Boccacci. *Introduction to Inverse Problems in Imaging*. Institute of Physics, Bristol, UK, 1998.
- [17] O. M. Bucci and T. Isernia. Electromagnetic inverse scattering: retrievable information and measurement strategies. *Radio Sci.*, 32:2123–2138, 1997.
- [18] R. P. Porter and A. J. Devaney. Generalized holography and computational solutions to inverse source problems. *J. Opt. Soc. Am.*, 72(12):1707–1713, 1982.
- [19] O. M. Bucci, L. Crocco, and T. Isernia. Improving the reconstruction capabilities in inverse scattering problems by exploitation of close-proximity setups. *J. Opt. Soc. Am. A*, 16:1788–1798, 1999.
- [20] A. Brancaccio, G. Leone, and R. Pierri. Information content of born scattered fields: results in the circular cylindrical case. *J. Opt. Soc. Am. A*, 15(7):1909–1917, 1998.
- [21] R. Pierri, R. Persico, and R. Bernini. Information content of the born field scattered by an embedded slab: multifrequency, multiview, and multifrequency-multiview cases. *J. Opt. Soc. Am. A*, 16(10):2392–2399, 1999.
- [22] O.M. Bucci, L. Crocco, T. Isernia, and V. Pascazio. Subsurface inverse scattering problems: quantifying, qualifying, and achieving the available information. *IEEE Transactions on*

- Geoscience and Remote Sensing*, 39(11):2527–2538, Nov 2001.
- [23] A. J. Devaney, E. A. Marengo, and M. Li. Inverse source problem in nonhomogeneous background media. *SIAM Journal on Applied Mathematics*, 67(5):1353–1378, 2007.
- [24] M. R. Khodja and E. A. Marengo. Radiation enhancement due to metamaterial substrates from an inverse source theory. *Physical Review E (Statistical, Nonlinear, and Soft Matter Physics)*, 77(4):046605, 2008.
- [25] S. Nordebo, M. Gustafsson, and B. Nilsson. Fisher information analysis for two-dimensional microwave tomography. *Inverse Problems*, 23(3):859–877, 2007.
- [26] M. Gustafsson and S. Nordebo. Cramer-Rao lower bounds for inverse scattering problems of multilayer structures. *Inverse Problems*, 22(4):1359–1380, 2006.
- [27] R. E. Collins. *Foundations for Microwave Engineering*. Mc-Graw Hill, New York, 1966.
- [28] R. Lencrerot, A. Litman, H. Tortel, and J.-M. Geffrin. Measurement strategies for a confined microwave circular scanner. *Inv. Probl. Sci. Eng.*, in print, 2009.
- [29] O. M. Bucci, N. Cardace, L. Crocco, and T. Isernia. Degree of nonlinearity and a new solution procedure in scalar two-dimensional inverse scattering problems. *J. Opt. Soc. Am. A*, 18(8):1832–1843, 2001.
- [30] O. M. Bucci, N. Cardace, L. Crocco, and T. Isernia. 2-d inverse scattering: degree of nonlinearity, solution strategies and polarization effects. In M. Fiddy and R. Millane, editors, *Image reconstruction from incomplete data*, , *Proc. SPIE vol.4123*. San Diego, 2000.